I&EC research
Industrial & Engineering Chemistry Research

Article

Cite This: Ind. Eng. Chem. Res. 2018, 57, 13300−13311

pubs.acs.org/IECR

Numerical Simulation of Biomass Growth in OKTOP®9000 Reactor at Industrial Scale

Dmitry Vladimirovich Gradov,*[,†] Mei Han,[†] Petri Tervasmäki,[‡] Marko Latva-Kokko,[§] Johanna Vaittinen,[∥] Arto Pihlajamäki,[†] and Tuomas Koiranen[†]

[†]School of Engineering Science, Lappeenranta University of Technology, P.O. Box 20, FI-53851 Lappeenranta, Finland
[‡]Chemical Process Engineering, University of Oulu, P.O. Box 4000, FI-90014 Oulu, Finland
[§]Outotec (Finland) Oy, Outotec Research Center, P.O. Box 69, FI-23101 Pori, Finland
[∥]Neste Engineering Solutions, NAPCON, P.O. Box 310, FI-06101 Porvoo, Finland

Supporting Information

ABSTRACT: Computational fluid dynamics is a powerful method for scale-up of reactors although it is still challenging to fully embrace hydrodynamics and biological complexities. In this article, an aerobic fermentation of *Pichia pastoris* cells is modeled in a batch OKTOP®9000 reactor. The 800 m^3 industrial scale reactor is equipped with a radial impeller, designed by Outotec Oy for gas dispersion in the draft tube reactor. Measured N_p of the impeller is used in hydrodynamics validation. The resolved energy dissipation rate is compensated, and its influence on mass transfer is analyzed and discussed. Gas−liquid drag force is modified to simulate effects of liquid turbulence and bubble swarms. Resolved steady state multiphase hydrodynamics is used to simulate the fermentation process. Temporal evolution of species concentrations is compared to experimental data measured in a small copy of the reactor at lab scale (14 L). The effect of oxygenation on the *P. pastoris* cells cultivation is considered.

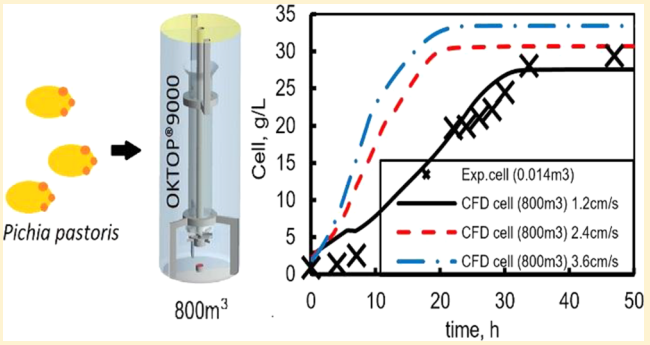

1. INTRODUCTION

Microbial cells are used to produce a wide range of products. In a majority of the production processes, microbes are aerobic and require oxygen for respiration and the cultivation is carried out in aqueous medium. Therefore, efficient oxygen transfer from gas to liquid phase is essential.[1] The industrially relevant reactor scales are tens or hundreds cubic meters, and these reactors cannot be approximated by an ideally mixed approach. As pointed out by Nauha et al.,[2,3] the gas handling capacity of stirred tank reactors (STR) often becomes one of the limiting factors in the large scale. Furthermore, flow patterns in STR with high aspect ratio—typical for large scale applications—often exhibit compartmentalization of the overall dispersion flow and limited axial recirculation throughout the reactor volume.[4]

The OKTOP®9000 reactor was originally developed for direct leaching of zinc concentrate during the 1990s. Today they are in use at some of the largest zinc production plants in the world with reactor volumes ranging around 1000 m^3. Gas-to-liquid mass transfer is an important issue also in hydrometallurgy due to low oxygen solubility and high oxygen demand. Several hydrometallurgical operations are controlled by the rate of oxygen transfer from gas to aqueous phase. Therefore, the OKTOP®9000 reactor is designed to have high gas-to-liquid mass transfer capacity and good oxygen utilization efficiency at relatively low agitation power costs. Thus, this type of reactor is also suitable for fermentation processes that require high gas−liquid mass transfer capacity. Gas−liquid mass transfer studies in this type of reactor have been published by Kaskiala[5] and Tervasmäki et al.[6]

For modeling the fermentation process, an accurate description of oxygen mass transfer is vital. Development of mass transfer formulation proposed in the literature can be followed since 1904, as it includes more features of physical mechanism and less assumptions.[7] Interfacial mass transfer is often described by surface renewal models out of which two groups can be distinguished, namely slip-velocity and eddy-cell models.[7−9] In turbulent flows, volumetric power describes the mass transfer more adequately than slip-velocity models.[9] However, the influence of ratio between available energy in fluid and contact surface area of bubbles is unknown[8] and given by empirical coefficient.

Computational fluid dynamics (CFD) has been widely used by researchers to simulate complicated multiphase systems with coupled chemical reactions.[10−15] Models describing gas−

Received: June 21, 2018
Revised: September 6, 2018
Accepted: September 10, 2018
Published: September 10, 2018

DOI: 10.1021/acs.iecr.8b02765
Ind. Eng. Chem. Res. 2018, 57, 13300−13311

liquid hydrodynamics are capable of predicting agitated fluid flow with fair accuracy. At a compromise of time and computational power available, multiphase reactor performance can be evaluated. Simulating of industrial-scale applications (hundreds of m^3) in a reasonably short time is not common; therefore, only a few relevant published works were found. The effect of spatial discretization on simulated results has to be mentioned here. Typically, reactor geometry does not require a high number of elements to resolve main flow features and simulation time is moderate. Unfortunately, this is not valid for energy dissipation rate which is known to be affected greatly by mesh size.[16] Lane[16] tested several turbulence models in lab scale stirred tank (72 L) at different grids and found that energy dissipation rate is resolved up to 90% at the grid of around 20 million mesh nodes that is not feasible in multiphase mixing simulations at industrial scale.

The local hydrodynamics and gas−liquid mass transfer rate from numerically resolving mass, momentum, and energy balance equations allow one to obtain more insight into assessing the reactor performance compared with empirical correlations for scale-up process of multiphase reactors. The empirical correlations are usually derived from laboratory or pilot-scale experiments where the characteristics of the substrate gradient and the gas−liquid mass transfer are different from the large scale mainly due to mixing heterogeneity.[17,18]

Lapin et al.[19,20] developed an Euler−Lagrange approach to characterize the lifeline/history of an individual cell and performed the simulations of fed-batch cultivations in stirred tank reactors for *Saccharomyces cerevisiae* (0.07 m^3) and *Escherichia coli* (0.9 m^3). The modeling work concentrated, among other things, on the detailed description of the sugar uptake of the cells as both of the example organisms are sensitive to glucose concentration in the environment, and concentration gradients are typically expected in fed-batch reactors with high glucose concentration in the feed. Morchain et al.[10] performed the simulation of STR fermenters with volume of 0.07 and 70 m^3, applying a Euler−Euler approach for gas−liquid flow and the population balance model (PBM) for microorganism heterogeneity. Haringa et al.[14] simulated the aerobic *S. cerevisiae* fermentation in a 22 m^3 fermenter where a large scale substrate concentration gradient exited due to competition between the mixing and the substrate uptake. In their work, the Eulerian−Eulerian approach was used for gas−liquid fluid flow, coupling with PBM to account for bubble size distribution. The discrete phase model with one-way coupling was employed for tracking the cell population and describing the bioreaction. They found that substrate was well mixed within each circulation zone originating from the individual Rushton turbine. The concentration gradient was noticed to be compartmentalized along the reactor. However, the scale of the industrial reactor very often needs to be hundreds of cubic meters to achieve a profitable bioprocess, which leads to a significant computational power requirement.[2] Therefore, accurate resolving of turbulence characteristics becomes challenging at large scale, which has a significant effect on the gas−liquid hydrodynamics and mass transfer. The interactions between microbial metabolism and environmental factors such as oxygen and/or substrate concentrations and mass transfer conditions may be complex. Therefore, the suitability of a certain reactor type and operational conditions for microbial cultivation should be estimated by using information on the microbial growth−not solely based on the information on the hydrodynamic conditions.

The aim of this research is to develop a CFD model for simulating cell cultivation in an industrial-scale OKTOP®9000 reactor. Using process equipment sizing data, a model was developed that is able to provide accurate results efficiently with respect to computing power and simulation time within feasible limits. Gas−liquid hydrodynamics, oxygen mass transfer, and yeast metabolism reactions are considered in the model. The effect of compensated volumetric power on gas−liquid mass transfer is studied. The aerobic cultivation of *Pichia pastoris* is simulated in batch mode. The effect of oxygen supply on the cells metabolism is considered.

2. MATERIALS AND METHODS

2.1. Metabolism of *Pichia Pastoris* Yeast. The description of growth kinetics is based on the model presented by Tervasmäki et al.[21] The model recognizes three different metabolic routes, which may be present when the yeast is grown on glucose. Glucose is utilized as the primary carbon source either by a respirative (eq 1) or fermentative (eq 2) route depending on the oxygen availability. Ethanol, which may be present as a product from alcoholic fermentation, can be utilized by respirative metabolism (eq 3) in the absence of the primary carbon source, glucose. The model has been developed and its parameters have been estimated based on literature sources. The specific reaction rates (q) and growth rates (μ) are presented by eqs 4−11.

$$C_6H_{12}O_6 + aO_2 + bNX[NH_3] \rightarrow bCH_{HX}O_{OX}X_{NX} + cCO_2 + dH_2O \quad (1)$$

$$C_6H_{12}O_6 + gNX[NH_3] \rightarrow gCH_{HX}O_{OX}X_{NX} + hCO_2 + iH_2O + jC_2H_6O \quad (2)$$

$$C_2H_6O + kO_2 + lNX[NH_3] \rightarrow lCH_{HX}O_{OX}X_{NX} + mCO_2 + nH_2O \quad (3)$$

$$q_g^{ox1} = \frac{\mu_{\max}^{ox}}{Y_{xg}^{ox}} \frac{c_g}{c_g + K_g} \frac{c_o}{c_o + K_o} \quad (4)$$

$$q_g^{ferm} = \frac{\mu_{\max}^{ferm}}{Y_{xg}^{OX}} \frac{c_g}{c_g + K_g} \left(1 - \frac{c_o}{c_o + K_o}\right) \quad (5)$$

$$q_e^{ox2} = \frac{\mu_{\max}^{e}}{Y_{xe}^{OX}} \frac{c_e}{c_e + K_e} \frac{K_i}{c_g + K_i} \frac{c_o}{c_o + K_o} \quad (6)$$

$$\mu_g^{ox} = q_g^{ox} Y_{xg}^{ox} \quad (7)$$

$$\mu_g^{ferm} = q_g^{ferm} Y_{xg}^{ferm} \quad (8)$$

$$\mu_e^{ox} = q_e^{ox} Y_{xe}^{ox} \quad (9)$$

$$q_o^{g} = q_g^{ox} Y_{og}^{ox} \quad (10)$$

$$q_o^{e} = q_e^{ox} Y_{xe}^{ox} \quad (11)$$

where q_i is the specific rate of component i ($g_i/(g_x \cdot h)$) and subscripts x, g, e, and o denote cells, glucose, ethanol, and oxygen, respectively. Superscripts *ox* and *ferm* in eqs 4−9

DOI: 10.1021/acs.iecr.8b02765
Ind. Eng. Chem. Res. 2018, 57, 13300−13311

Figure 1. Industrial scale OKTOP®9000 reactor (left) (Outotec Plc., n.d.[22]) and CAD geometry for large-scale reactor and impeller (right). Credit line: Adapted with permission from http://www.outotec.com/products/leaching-and-solution-purification/zinc-concentrate-direct-leaching. Copyright Outotec Oyj 2018.

denote respirative and fermentative metabolism, and superscripts g and e in eqs 10−11 denote oxygen consumption due to glucose and ethanol utilization, respectively. Parameters μ_{max}, Y, and K are listed in Table S1. Details of the model and validation with laboratory scale experiments are presented in Tevasmäki et al.[21]

2.2. OKTOP®9000 Reactor. The OKTOP®9000 reactor has been developed for direct leaching of zinc concentrate in atmospheric conditions. This proven technology applied in industry globally provides the following positive features: high oxygen mass transfer capacity and oxygen utilization efficiency, moderate mixing power requirement, and low mixing time. The OKTOP®9000 reactor is presented at industrial scale in Figure 1. Three baffles are mounted to the vessel walls in the down part of the reactor in order to prevent flow circulation and promote mixing. Designed by Outotec, the stirrer is a combination of a hydrofoil impeller and a radial turbine. The upper parts of the blades are rounded to create high flow and fluid circulation inside the reactor whereas the down parts are made straight to disperse and distribute gas radially. The outer corners of the blades are trimmed to fit the draft tube and reduce the power number of the impeller. The stirrer clearance is 0.33T. A ring-sprager is mounted below the impeller. The ring has a square profile with replaceable upper lid that is perforated as needed. The lid surface (≈ 0.9 m^2) of the ring-sparger is perforated uniformly with holes of 1 mm in diameter. The dimensions of the reactor are presented in Table S2. The liquid aspect ratio is set around 3.

For the model validation purposes, the computational domain of the large-scale reactor is built based on scale-up of an existing laboratory scale test device. The main constructive differences between the industrial device and CFD model are in shaft orientation (bottom versus top entry) and draft tube support frames arrangement. These changes are not supposed to affect the overall hydrodynamics.

2.3. Operational Conditions of Batch Cultivation of *P. Pastoris*. The batch cultivation of the yeast has been performed experimentally at the lab scale OKTOP®9000 reactor by Tervasmäki et al.[21] The volumetric power and aeration rate used in the lab scale tests were maintained when scaling-up the process to a 800 m^3 reactor. The operational conditions during the cultivation are summarized in Table S3.

In CFD simulations, the aeration rate was varied to study the effect of oxygenation on the bacteria metabolism. Maximum air flow rate was limited by the flooding at the chosen mixing speed.

2.4. Numerical Approach. *2.4.1. Simulation Strategy.* The modeling was carried out in ANSYS Fluent 18 by a

DOI: 10.1021/acs.iecr.8b02765
Ind. Eng. Chem. Res. 2018, 57, 13300−13311

Scheme 1. Block Scheme of Numerical Approach Used in This Work

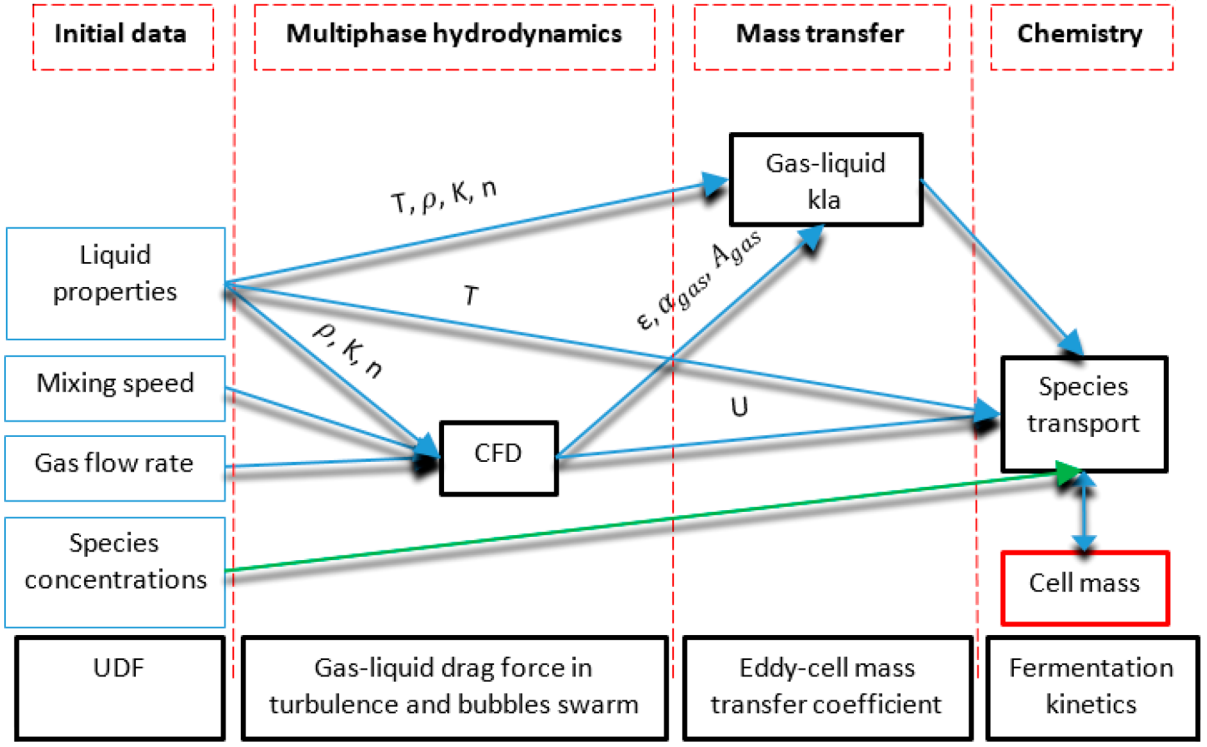

standard tool kit of the software package with partial usage of user defined function (UDF) when customization was needed. Scheme 1 presents a block-scheme of the simulation strategy used in this work. The overall strategy is divided in four parts entitled by names in red dashed squares. Initial properties of the solution of the cell cultivation process are used to calculate multiphase mixing hydrodynamics in the reactor. Gas−liquid mass transfer is found via postcalculation from the results of the resolved hydrodynamics at steady state. Biological activities are then simulated using data from the simulated hydrodynamics, oxygen mass transfer, and initial species concentrations.

2.4.2. Multiphase Fluid Flow. The volume averaged Stoke's number (eq 12) for the studied system is around 11, meaning that the gas phase influence on the liquid phase is not negligible and it has to be taken into account.

$$St = \frac{\tau_p}{\tau_q} = \frac{d_p^2 \varepsilon^{0.5}}{36\nu^{1.5}} \tag{12}$$

where τ_p and τ_q are the relaxation time of the primary phase and bubble, s, d_p is the bubble diameter, m, ε is the energy dissipation, m^2/s^3, and ν is the kinematic viscosity, m^2/s.

Therefore, the Eulerian−Eulerian multiphase approach was used to simulate gas−liquid flow, in which gas and liquid phases are considered as interpenetrating continua expressed via volume fraction per phase and the mass balance is controlled by eq 13. A set of conservation equations is solved for each phase (eqs 14 − 15).

$$\sum_i \alpha_i = 1 \tag{13}$$

$$\nabla \overline{u} = 0 \tag{14}$$

$$\overline{u}\cdot\nabla\overline{u} = -\nabla\overline{p} + \nabla\cdot[(\mu + \mu_{turb})\nabla\overline{u}] \tag{15}$$

where α_i is the phase volume fraction, $\overline{u}$ a phase velocity, m/s, $\overline{p}$ is the pressure, Pa, and μ and μ_{turb} are the laminar and turbulent viscosities, Pa·s.

2.4.3. Turbulence. It was desired to develop a model that is able to provide results efficiently with respect to computing power and time, for which reason it was decided to apply a Reynolds-averaged Navier-Stoke's (RANS) turbulence model in the current simulations. Turbulence formulations in RANS models are based on statistical analysis rather than on actual physical phenomena. In our previous work,[23] three popular models in the RANS family were tested, namely the Realizable k-ε model, the shear stress transport k-ω model (k-ω SST), and the Reynolds stress model (RSM). The Realizable k-ε model produced the most accurate results for single and multiphase mixing in round-bottom STR and has therefore been applied in this work.

$$\overline{u}\cdot\nabla k = P - \varepsilon + \nabla\cdot\left[\left(\mu + \frac{\mu_{turb}}{\sigma_k}\right)\nabla k\right] \tag{16}$$

$$\overline{u}\cdot\nabla\varepsilon = C_{\varepsilon 1}\frac{\varepsilon}{k}P - C_{\varepsilon 2}\frac{\varepsilon^2}{k}P + \nabla\cdot\left[\left(\mu + \frac{\mu_{turb}}{\sigma_\varepsilon}\right)\nabla\varepsilon\right] \tag{17}$$

where k is the turbulence kinetic energy, m^2/s^2.

The dispersed turbulence formulation model was used since the secondary phase is dilute and fluctuating quantities of the gaseous phase may be found as the function of the mean terms of the liquid phase. At first, turbulence terms k and ε are computed for the primary phase. Then, secondary phase turbulence terms are found and exchange of turbulence momentum between phases is computed based on Tchen-theory.[24]

2.4.4. Phase Interaction. Gradov et al.[23] showed that the Schiller−Naumann's drag force model in conjunction with

DOI: 10.1021/acs.iecr.8b02765
Ind. Eng. Chem. Res. 2018, 57, 13300−13311

Lane's turbulence modification factor gave the most accurate results for air−water mixing in a stirred tank at the assumption of constant bubble diameter equal to 1 mm. Also, the effect of nondrag forces was found insignificant. Therefore, in order to reduce computational complexity and promote solution stability, the above-mentioned combination of models was used to simulate drag force, while other force models were ignored. The momentum conservation eq (eq 18) includes the cumulative force $\vec{F}_q$ (eq 19) acting on the primary phase.

$$\frac{\partial}{\partial t}(\alpha\rho\vec{u})_q + \nabla\cdot(\alpha\rho\vec{u}\vec{u})_q = \nabla\cdot(\alpha\sigma)_q - \alpha_q\nabla p + \vec{F}_q + \alpha_q\rho_q\vec{g} \tag{18}$$

$$\vec{F}_q = \sum_{p=1}^{n}(K_{pq}(\vec{u}_p - \vec{u}_q) + \dot{m}_{pq}\vec{u}_{pq} - \dot{m}_{qp}\vec{u}_{qp}) \tag{19}$$

Different drag models can be found in published literature. The most popular model, proposed by Schiller and Naumann[25] in eq 21, is a drag model suitable for rigid spherical particles.

$$K_{pq} = \frac{\rho_p C_D \mathrm{Re}}{144\tau_p} d_p A_i \tag{20}$$

where ρ_p is the particle density, kg/m^3, C_D is the drag force coefficient, Re is the relative Reynolds number, and A_i is the interfacial area, m^2. The drag force coefficient is the function of Re according to the following formulation:

$$C_D = \begin{cases} 24(1 + 0.15Re^{0.687}) & Re \le 1000 \\ 0.44 & Re > 1000 \end{cases} \tag{21}$$

The drag force model is based on bubble rise velocity measured in stagnant fluids, which is higher than rise velocity in turbulent flow. A model correcting drag force coefficient for turbulence was proposed by Brucato et al.[26] at first. This turbulence modification factor concept (eq 22) changes stagnant fluid drag force to make it suitable for adoption in turbulent multiphase flow simulation. Later, Lane et al.[27] suggested a new correlation (eq 23) for turbulence modification factor that is based on ratio of stagnant to turbulent terminal velocity $\frac{U_s}{U_T}$ to be correlated with ratio of particle relaxation time to integral time scale of turbulence.

$$K'_{pq} = \eta K_{pq} = \left(1 + K\left(\frac{d_p}{\lambda}\right)^3\right)K_{pq} \tag{22}$$

where η is the turbulence modification factor, $K = 6.5 \times 10^{-6}$ and λ is the Kolmogorov length scale, m.

$$\eta = \left(1 - 1.4\left(\frac{\tau_p}{T_L}\right)^{0.7} e^{(0.6\tau_p/T_L)}\right)^{-2} \tag{23}$$

$$T_L = 0.135\frac{k}{\varepsilon} \tag{24}$$

The presence of a bubbles swarm reduces liquid flow energy increasing drag force between phases. The effect of gas volume fraction (0.01−0.45) of dispersed gas onto gas−liquid drag force has been modeled by Roghair et al.[28] in the flows of intermediate and high Reynolds number as

$$C_{D,swarm} = C_D\left(1 + \alpha_p\left(\frac{18}{E\ddot{o}}\right)\right)(1 - \alpha_p) \tag{25}$$

where $E\ddot{o}$ is the Eötvös number, which is a dimensionless number to characterize the shape of bubbles or drops moving in a surrounding fluid.

2.4.5. Mass Transfer. According to the eddy-cell model, mass transfer is described as a function of energy dissipation rate and rheological parameters defining micromixing.[9] With the assumption of constant temperature, local energy dissipation determines the mass transfer coefficient according to eq 26 as suggested by Kawase and Moo-Young:[29]

$$k_L = C\sqrt{D_L}\left(\frac{\varepsilon\rho}{K}\right)^{1/[2(1+n)]} \tag{26}$$

where D_L is the gas diffusivity in liquid, m^2/s (2.26×10^{-9}, Han and Bartels[30]), ρ is the liquid density, kg/m^3, K is the consistency index, Pa·s^n, n is the dimensionless flow behavior index, and C is the proportionality coefficient. The effect of gas bubbles on the mass transfer coefficient is taken into account with the proportionality coefficient. The value of 0.301 for the coefficient, proposed by Kawase and Moo-Young,[29] has been tested by Garcia-Ochoa and Gomez[31] and was found to produce accurate results for gas−liquid mass transfer in stirred bioreactors.

The specific volumetric surface area of the secondary phase is found as follows:

$$A_p = \frac{6\alpha_p}{d_p} \tag{27}$$

Calderbank et al.[32] proposed a correlation for Sauter mean diameter of bubbles in alcohol solutions:

$$d_{32} = 1.9\left(\frac{\sigma^{0.6}}{\varepsilon^{0.4}\rho^{0.6}}\right)\left(\frac{\mu_{gas}}{\mu_L}\right)\alpha_p^{0.65} + 0.0009 \tag{28}$$

where σ is the surface tension, N/m. The surface tension of the water−ethanol (1%) solution was measured and resulted in 0.069 N/m.

Machon et al.[33] tested solutions of various gas−liquid surface tension in a stirred tank at three different vertical locations by recording bubble sizes. They concluded mean bubble size as a function of surface tension and specific volumetric mixing power. Based on the results presented, mean bubble size is 2 mm in 1% water−ethanol solution. Later, Hu et al.[34] tested gas−liquid solutions of various surface tensions in turbulent flow and proposed a correlation for Sauter mean bubble size, predicting similar bubble size (2 mm) in OKTOP®9000.

2.4.6. Bacterial Activity. The conservation equation of species transport in turbulent flow is as follows:

$$\frac{\partial}{\partial t}(\rho Y_i) + \nabla\cdot(\rho\vec{u}Y_i) = \nabla\cdot(\rho(D_{i,m} + D_t)\cdot\nabla Y_i) + R_i \tag{29}$$

where Y_i is the mass fraction of component i, $D_{i,m}$ and D_t are the diffusivities due to laminar and turbulence diffusion correspondingly, m^2/s, and R_i is the net rate of production of species i by chemical reaction kg/(m^3·s).

Haringa et al.[14,15,35] found significant concentration gradients at $Da \approx 50$ along the tall reactor equipped with four Rushton turbines, compartmentalized them, and performed a scale-down simulator design from CFD data.

DOI: 10.1021/acs.iecr.8b02765
Ind. Eng. Chem. Res. 2018, 57, 13300−13311

However, such concentration gradients are negligibly small ($Da \approx 5$) in OKTOP®9000 at the studied operational conditions. Therefore, the method is not feasible in this work. Net reaction rates of the species are modeled via UDF as a source term.

$$R_i = -(q_i^{ox1} + q_i^{ferm} + q_i^{ox2})c_x \quad (30)$$

$$R_x = -(\mu_g^{ox1} + \mu_g^{ferm} + \mu_e^{ox2})c_x \quad (31)$$

$$R_o = k_L a(c_o^{sat} - c_o) - (q_o^{ox1} + q_o^{ox2})c_x \quad (32)$$

$$c_o^{sat} = \frac{M_o w_o (p_h - p_{vapor})}{k_H} \quad (33)$$

where i denotes a species, c_o^{sat} is the oxygen saturation concentration in the liquid phase, g/L; c_o is the oxygen concentration in the liquid phase, g/L; c_x is the biomass concentration, g/L; p_h is the hydrostatic pressure, atm; p_{vapor} is the vapor pressure (0.0419 at 30 °C according to Lide et al.[36]), atm; k_H is the Henry's constant (770), atm·L/mol; w_o is the mass fraction of oxygen, and M_o is the molar weight of oxygen, g/mol.

2.4.7. Boundary Conditions, Solver Settings, and Convergence Criteria. Mixing in the draft tube reactor was modeled using the multiple reference frame (MRF) method where the rotor is fixed, around which the fluid in the mixing zone is rotated. The method allows steady state simulation at accuracy comparable to the sliding mesh (SM) method as proved by Joshi et al.[37] In the works published previously,[23,38] the MRF approach in combination with the Realizable k-e turbulent model simulated flow characteristics in a STR accurately close to PIV measurements. Moreover, the results of the sliding mesh approach are not sufficiently verified in turbulent and multiphase mixing flows.[37]

Near wall flow was modeled using a standard wall function due to simplicity and varying y+ value along the walls of the draft tube reactor. Therefore, the grids were made such that the elements next to the wall fell into the range 30−300 of y+ value.[39]

In the CFD simulations, the stirred tank can be considered as a semibatch system where gas, supplied via sparger, exits through the liquid surface. The boundary conditions are schematically presented in Figure 2.

At first, the liquid phase mixing flow field has been simulated. Then, in order to reduce computational instabilities, the simulation was switched to transient state (time step is 0.02 s) and gas was fed until mass balance criteria (5% deviation) was met and gas−liquid hydrodynamics stabilized. Under relaxation factors of pressure and velocity were reduced up to 0.15 and 0.35 correspondingly to facilitate convergence. A second order discretization scheme was applied to all the solved variables. The convergence criterion was set at 10^{-4} for all the calculated variables. When multiphase flow hydrodynamics have been computed, mass transfer was calculated on top of multiphase results according to eqs 26−27. Species transport equations were solved at frozen gas−liquid hydrodynamics.

2.4.8. Spatial Resolution. Spatial discretization is known to affect simulation results as mentioned earlier in section 1. At feasible grid size, energy dissipation, which is an important parameter influencing bubble size, mass transfer coefficient etc., is underestimated in STRs already at lab scale, not

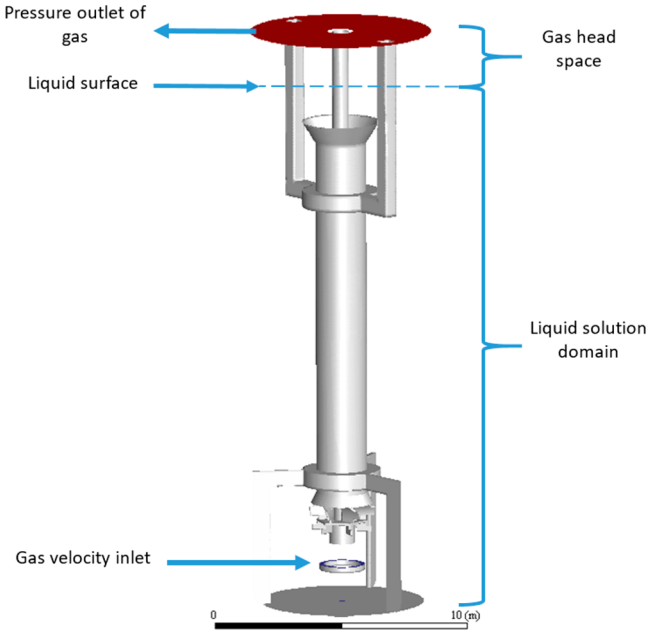

Figure 2. Schematic presentation of boundary conditions to simulate gas−liquid mixing.

mentioning pilot and industrial ones.[16,37] Therefore, refining a grid of the reactor of large scale would result in an enormous number of cells, which is not practical. The computational grid test carried out in this study had a purpose to preserve the main flow field features resolved such as liquid velocity and surface stress on the impeller. The mesh in the stationary zone was meshed by structured elements while the region around the impeller composed unstructured ones (Figure 3). Four grids were produced by doubling the number of elements.

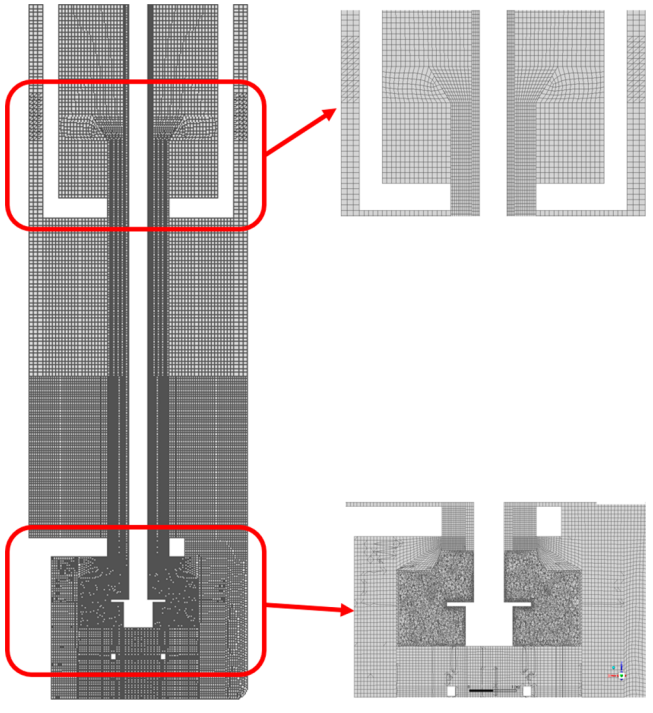

Figure 3. Example of spatial discretization (grid 3) in vertical slice.

DOI: 10.1021/acs.iecr.8b02765
Ind. Eng. Chem. Res. 2018, 57, 13300−13311

The grid test (Table S4) was performed using single phase mixed at 60 rpm. Out of the results, grid 3 with 2 million elements was chosen as an optimal one in further simulations.

2.4.9. Post Processing of Simulation Results. Power number (N_p) measured at an industrial OKTOP®9000 reactor was shared by Outotec Co for validating the large-scale CFD model (see section 2.2). The simulated power number was within 8% difference to N_p measured in the large scale reactor. From the model, the power draw can be expressed via energy dissipation integrated over the vessel volume according to the following expression:

$$P_\tau = 2\pi N \int \tau dA_{imp} \tag{34}$$

$$P_\varepsilon = \rho \int \varepsilon dV \tag{35}$$

where P is the power draw, W, N is the mixing speed, s^{-1}, τ is the stress, Pa, A_{imp} is the impeller area, m^2, and V is the volume of reactor, m^3.

Due to the usage of a head space in the simulations (see Figure 3), the global values of mixing power, gas hold-up, and gas−liquid mass transfer were calculated from the iso-surface based on the gas hold-up range 0−0.5. It is worth mentioning that a small region of high gas fraction in the vicinity of the gas sparger is not included into the iso-surface.

3. RESULTS

The used models and boundary conditions in the current multiphase mixing simulations are summarized in Table S5.

The simulations were performed using 8 cores of Intel(R) Core(TM) i7-7700 CPU @3.60 GHz and 16Gb operational memory. The strategy comprised three steps, namely: single phase mixing in steady state (7 eq-s−10 s/iteration), transient gas−liquid mixing (14 eq-s−20 s/iteration), and fermentation (5 eq-s−6s/iteration), which took 10 days of calculations for a set of operational conditions.

3.1. Reactor Hydrodynamics. In Figure 4, the velocity vector field in a vertical plane is presented where all vectors are of the same size and in-plane to show the overall flow field in single phase mixing at 1 s^{-1}.

The draft tube enlarges the upper circulation loop, produced by a radial impeller. This effect combines benefits of airlift and stirred tank reactors. With a single mixer, aerated gas is well-distributed in the OKTOP®9000 reactor producing a large gas−liquid contact area while the raiser part provides a longer contact time. Depending on mixing speed, supplied gas can be trapped longer, being dragged into the draft tube near the reactor top. At strong enough agitation, solution can be aerated also through vortex appeared on the liquid surface. Global Da is smaller in single radial impeller draft tube reactors compared to multiple impeller reactors equipped with several Rushton turbines, which prevents compartmentalization of the species concentration gradient.[14]

The reactor aeration was simulated transiently and the global parameters such as volumetric power, gas−liquid contact area, and mass transfer were followed to ensure stable multiphase flow is achieved. Temporal evolution of global parameters traced was noticed to approach a stable level at 40 s of simulation time.

It is known that the mixing power estimated from simulations is calculated more accurately via torque (eq 34) than via the energy dissipation rate (eq 35).[16] The difference at

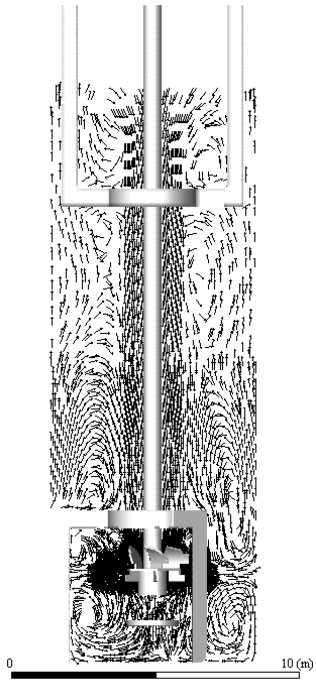

Figure 4. Velocity vector field of single phase water mixing at steady state in a vertical plane in the OKTOP®9000 reactor at 1 s^{-1} agitation speed.

steady state is around 20%, which goes along with the obseravtions made by Joshi et al.[37] and Lane.[16] The underpredicted ε can be compensated linearly by the coeffcient as follows:[40]

$$\beta = \frac{\varepsilon_{CFD,i}}{\sum_{i=1}^{NB} \varepsilon_{CFD,i} w_i} \tag{36}$$

$$\varepsilon^* = \beta \frac{P_\tau}{m_q} \tag{37}$$

where $\varepsilon_{CFD,i}$ is the local average energy dissipation rate calculated by CFD, m^2/s^3, w_i is the mass fraction of liquid in cell i, ε^* is the compensated energy dissipation rate, m^2/s^3, and m_q is the mass of liquid in cell i, kg.

At the assumption of constant bubble size, the k_La values in the rotating and stationary zones of the reactor obtained in this work are 26 and 84% of total mass transfer. The linearly compensated energy dissipation rate as $(1.2\varepsilon)^{0.25}$ increases the overall mass transfer coefficient less than 5%. One may debate that linear compensation is quite a guess and it should be performed rather via power law.[41,42] Checking this statement is worth separate research, and it is left out of the scope in this work. However, at the assumption that the underpredicted energy is located in the rotating zone, the linear compensation of ε in that zone only contributes to the overall k_L just around 2%. Thus, the mass transfer underprediction within 2−5% is negligible for the case under consideration at the assumption of constant bubble size.

More detailed information on the performance of the OKTOP®9000 reactor can be achieved from the contours of velocity filed, d_{32}, and specific mass transfer, presented in Figures 5−7. The effect of gas onto liquid phase hydrodynamics can be seen in Figure 5 where single and multiphase mixing hydrodynamics is presented in vertical midsection.

DOI: 10.1021/acs.iecr.8b02765
Ind. Eng. Chem. Res. 2018, 57, 13300−13311

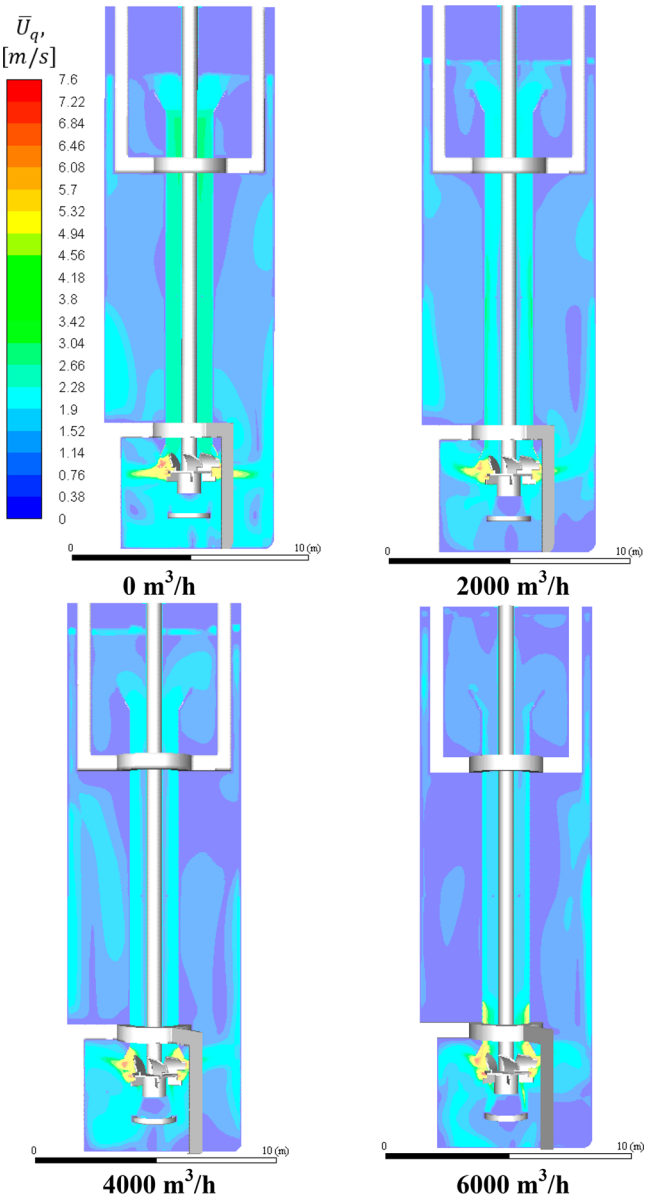

Figure 5. Steady state liquid phase velocity contours in vertical plane gas−liquid mixing in OKTOP®9000 reactor at different air flow rates.

The radial jets coming from the impeller are mainly pushes upward by gas, which reduces the mean velocity of the flow below the impeller. The mean velocity filed in the riser part of the reactor is almost unaffected while it is reduced in the draft tube due to the presence of gas. Near the solution surface, fluid is more agitated by gas escaping the liquid.

Gas−liquid hydrodynamics have been simulated with the assumption of constant bubble size, which is acceptable in the case of narrow BSD. However, mass transfer is much more sensitive toward bubble size. Therefore, eq 28 has been applied to get the Sauter mean diameter of bubbles in computational cells (Figure 6). Mean volumetric bubble size was around 1.7 mm in the case of 4000 m^3/h of gas flow rate, which produced 15% higher k_La. The calculated d_{32} has its minimum in the most turbulent region of radial flow created by the impeller while maximum values can be found in the regions of high local gas hold-ups and low mixing intensity that are located under impeller radial jet and in the central area close to the reactor top. Having left the mixing zone, the bubbles are moving spirally to the top staying distributed, which keeps relatively constant local gas volume fraction. As a result, no active coalescence can be seen in the middle of the reactor. At the top of the reactor, lowered mixing intensity in combination with increased gas hold-up results in coalescence rate increase and bubbles growth.

Additionally, the bubble size distribution was calculated at 4000 m^3/h to assess the prediction found by eq 28. For this purpose, the population balance equation for four moments represented the total number m_0, length m_1, surface area m_2, and volume m_3 of the population. The bubble size was limited in the range of 0.1−10 mm. Breakage frequency and daughter bubble distribution have been simulated using Laakkonen's models.[43] Coalescence was calculated via Luo's model.[44] The moments were calculated at frozen hydrodynamics using QUICK scheme and converged at 10^{-4}. The results of the calculated mean bubble size are summarized in Table S6.

The results state that the value of mean bubble size predicted by different methods produced close results. The higher the gas flow rate, the smaller the effect of the global mass transfer. Bubble size distribution, calculated via eq 28, was used further to get local mass transfer (Figure 7) and during the fermentation simulations.

Comparing the contours of specific mass transfer (Figure 7), similarity in distribution can be found; however, mixing at micro scale promoted by turbulence, where oxygen is transported from bubble to liquid, is higher in the down part of the reactor. The highest mass transfer is in the vicinity of the impeller. Few words should be said about gas−liquid mass transfer in the draft tube. During experimental tests of gas−liquid mixing in the OKTOP®9000 reactor, gas was noticed to separate from the liquid phase and stick to the shaft in the draft tube under the Coriolis forces. Thus, gas−liquid mass transfer can only take place via the slip-velocity mechanism and considering gas phase as dispersed in the draft tube is not justified. However, the input to k_La in the draft tube is insignificantly small as well as in the area near the liquid surface.

Tervasmäki et al.[21] studied lab scale version of OKTOP reactor over the range of gas flow rate and impeller speeds. In Chart 1, the comparison of the global gas−liquid mass transfer measured experimentally in the small scale reactor against simulated results at the industrial scale is presented.

Large reactors provide higher specific interfacial area as bubble size distribution remains similar to smaller reactors when scale-up is done based on constant volumetric power. As a result, the efficiency of oxygen transfer grows along with the scale of the OKTOP reactor at similar specific power input.

The industrial scale reactor is more than 20 m in height and operates under atmospheric pressure. High hydrostatic pressure increases oxygen saturation concentration in the reactor (Figure 8).

Microorganisms are sensitive to high shear strain of fluid media; therefore, the safety of *P. pastoris* bacteria was verified in the reactor at large scale. According to the electronic database of Harvard University,[45] the *P. pastoris* dimension is of 5 μm. In mixed flow, the turbulent eddies of size smaller than the bacteria can be of potential damage. Therefore, the ratio of the bacteria length to Kolmogorov's length scale is presented as a contour in a vertical plane (Figure 9) at 4000 m^3/h.

The areas of λ_x/η_K higher than 1 are potentially dangerous to the microorganisms. As can be seen, the flow strength is not

DOI: 10.1021/acs.iecr.8b02765
Ind. Eng. Chem. Res. 2018, 57, 13300−13311

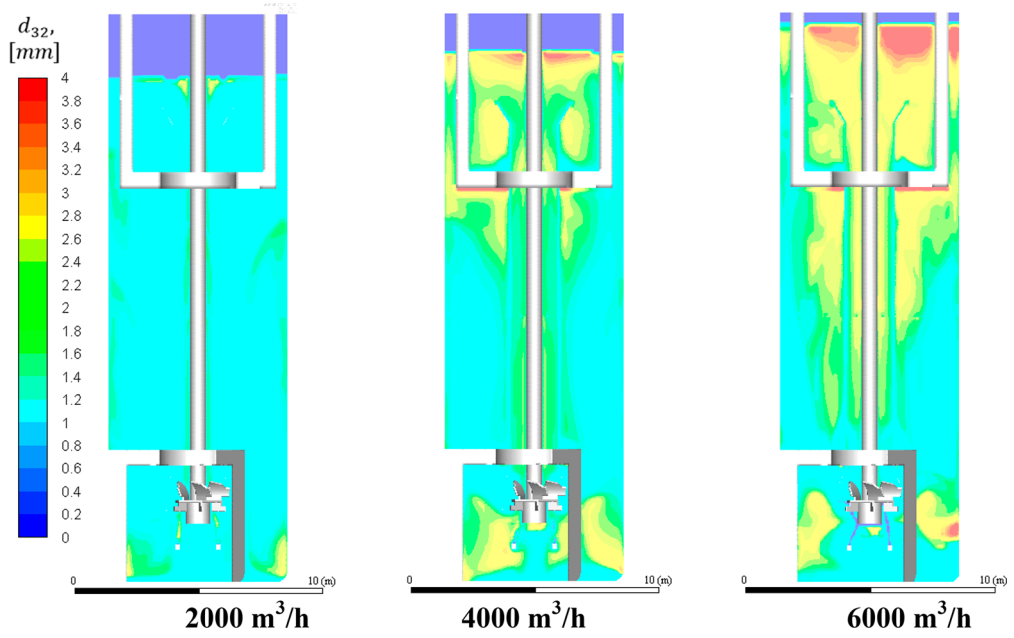

Figure 6. Contour of d_{32} in vertical plane in OKTOP®9000 reactor at different air flow rates and 1 s^{-1} calculated via eq 28.

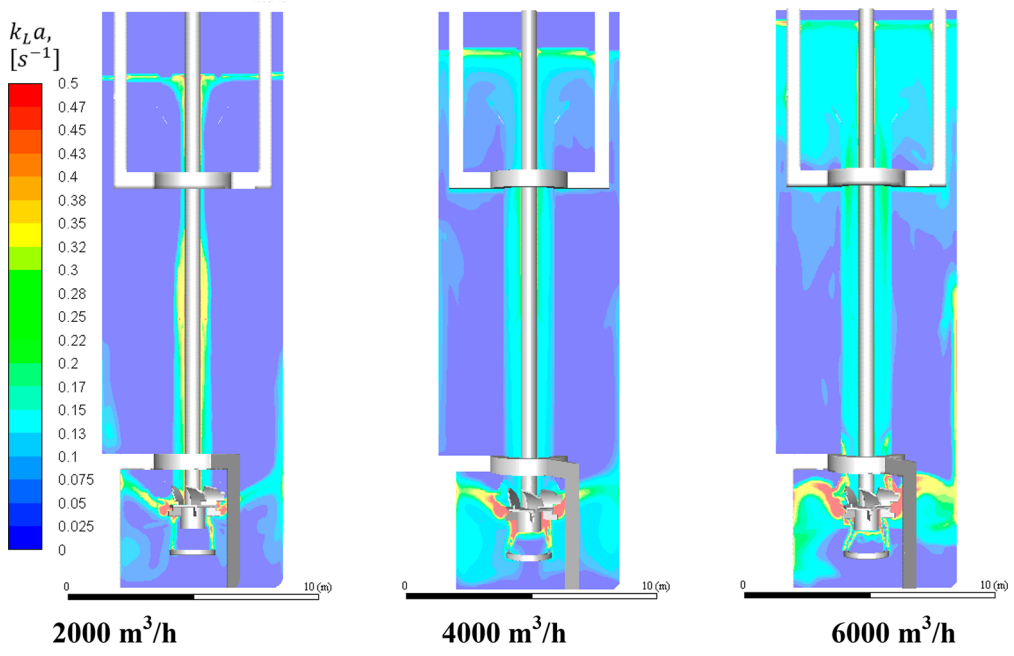

Figure 7. Contours of gas−liquid mass transfer in an OKTOP®9000 reactor at different air flow rates.

enough to harm the bacteria. However, further increase of mixing speed may affect the microorganisms.

3.2. Bio Reaction. *3.2.1. Batch Mode.* In this work, the cell cultivation process in the OKTOP®9000 reactor, initially enriched with oxygen, has been simulated in batch mode at 80 g/L of glucose and 2 g/L of cells. To verify the large-scale CFD results, experimental data was taken from the lab scale tests carried out by Tervasmäki et al.[21] for a similar but smaller setup. The concentrations of the glucose, ethanol, and cells are presented in Chart 2 as a function of time. The reported large-scale data points from CFD simulations were calculated as volume averaged.

The simulated results of the fermentation taking place in the reactor at large-scale (800 m^3) are in a reasonable agreement with those obtained during the experimental tests on the fermentation carried out in the OKTOP reactor at lab scale (14 L). Since the reaction rate is very low, the main difference between the reactors at lab and large scales is the oxygen transfer rate and oxygen saturation concentration. Following the ethanol production, the effect of oxygen transfer rate can be observed. Excess of available dissolved oxygen promotes glucose oxidation and inhibits fermentative reaction. Being converted to ethanol and then oxidized, the glucose loses part of its mass to CO_2, resulting in the reduction of cell yield. The conversion is faster at higher oxygen mass transfer rate as well. In addition, minor uncertainties in measurements and maintenance of operational conditions took place as well and

DOI: 10.1021/acs.iecr.8b02765
Ind. Eng. Chem. Res. 2018, 57, 13300−13311

Chart 1. Mass Transfer in OKTOP Reactors at Different Scales in Ethanol 1% Solution at P/V ≈ 500 W/m^3[a]

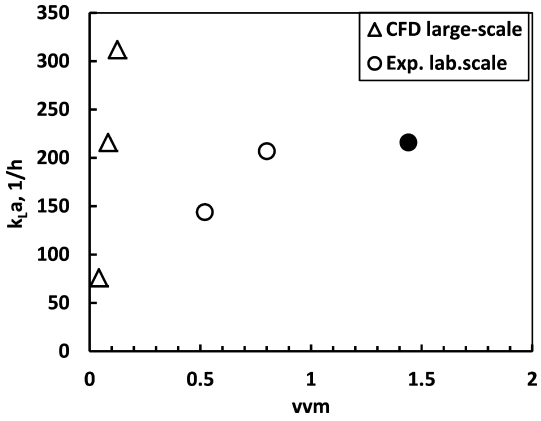

[a]Filled symbol corresponds to the experimental fermentation case in the lab-scale OKTOP reactor. Experimental data is from Tervasmäki et al.[21].

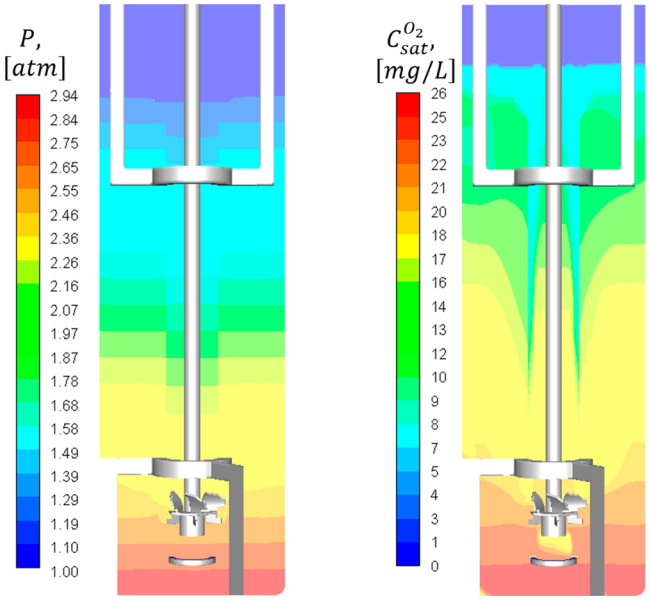

Figure 8. Contours of hydrostatic pressure (left) and oxygen saturation concentration (right) in the OKTOP®9000 reactor.

caused the deviation between simulated and experimental results.

4. CONCLUSIONS

This work presents an aerobic fermenter modeled at industrial scale. Multiphase mixing flow hydrodynamics was simulated at steady state in the draft-tube OKTOP®9000 reactor. Gas–liquid drag force, comprising effects of laminar, turbulent regimes and bubble swarms, was applied to model the behavior of gas bubbles in ethanol containing fluid. Power number was measured at large scale in single phase mixing tests, and it was used for the model validation.

The effect of linearly compensated energy dissipation (ε), caused by spatial discretization, onto gas–liquid mass transfer at narrow BSD is considered and found below 5% in the stirred reactor. However, compensated dissipated energy would have greater effect in cases of wide BSD as gas–liquid contact area grows and bubble size gets smaller in the regions of high ε and

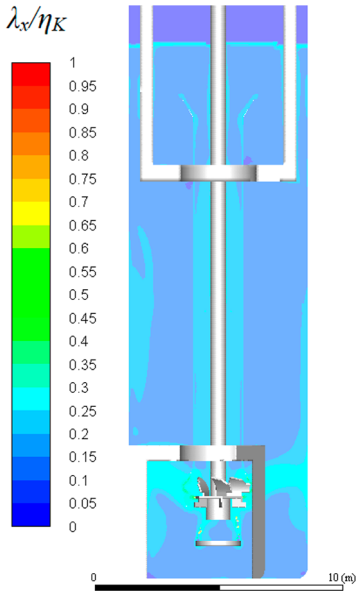

Figure 9. Contour of λ_x/η_K in a vertical plane in an OKTOP®9000 reactor at 1 s^{-1} and 4000 m^3/h.

Chart 2. Temporal Evolution of Normalized Concentration of Species in Batch OKTOP®9000 Reactor at 80 g/L of Glucose and 2 g/L of Cells[a]

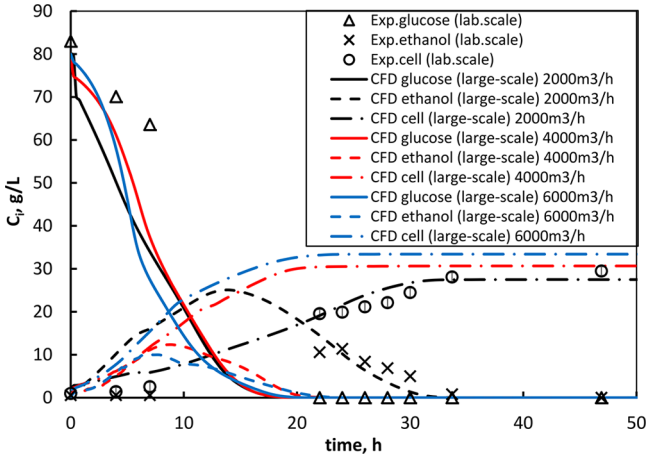

[a]Experimental data is from Tervasmäki et al.[21]

opposite trends take place in the regions of low dissipated energy.

The large scale OKTOP reactor provides higher oxygen mass transfer rate at similar volumetric power consumption as in the lab scale reactor due to higher specific interfacial area. BSD contributes up to 15% of total k_La compared to constant bubble size in 1% ethanol solution in the large scale OKTOP reactor.

Fermentation kinetics, describing metabolism of *Pichia pastoris* bacteria, is presented. The batch fermentation process of the cell cultivation was simulated in the draft tube stirred-tank reactor of industrial scale at different air supply rates. The results were compared with experimental data measured at similar reactor of lab scale, and a good match was found. At higher aeration rate, glucose fermentation is avoided, which cuts the carbon losses in CO_2 and increases the yield of the cells. The metabolism is pushed toward glucose oxidation that

DOI: 10.1021/acs.iecr.8b02765
Ind. Eng. Chem. Res. 2018, 57, 13300–13311

reduces retention time. The CFD modeling was proved to be a reliable tool for design of industrial aerobic fermenters.

■ ASSOCIATED CONTENT

Supporting Information

The Supporting Information is available free of charge on the ACS Publications website at DOI: 10.1021/acs.iecr.8b02765.

Table 1. *Pichia pastoris* cultivation kinetics parameters. Table 2. Sizing of OKTOP®9000 reactor at industrial scale. Table 3. Operational conditions of protein growth in lab scale OKTOP®9000 reactor. Table 4. Results of grid test of single phase mixing in OKTOP®9000 at 1 s^{-1}. Table 5. Summarized conditions for gas−liquid mixing in OKTOP®9000. Table 6. Volumetric mean d_{32} of bubbles found with different approaches and the corresponding mass transfer values (PDF)

■ AUTHOR INFORMATION

Corresponding Author

*Tel.: +358 46 5470573. E-mail addresses: dmitry.gradov@lut.fi, gradov-dmitrii@inbox.ru, dmitry.vladimirovich.gradov@gmail.com (D.V. Gradov).

ORCID

Dmitry Vladimirovich Gradov: 0000-0003-4222-0354

Notes

The authors declare no competing financial interest.

■ ACKNOWLEDGMENTS

The authors are grateful to the Finnish Funding Agency TEKES and, in particular, to Outotec Finland Oy and Neste Engineering Solutions Oy collaborating under FERMATRA project (908/31/2016 and 958/31/2016), for active supervision and financial support.

■ REFERENCES

(1) Garcia-Ochoa, F.; Gomez, E. Bioreactor Scale-up and Oxygen Transfer Rate in Microbial Processes: An Overview. *Biotechnol. Adv.* **2009**, *27* (2), 153−176.

(2) Nauha, E. K.; Visuri, O.; Vermasvuori, R.; Alopaeus, V. A New Simple Approach for the Scale-up of Aerated Stirred Tanks. *Chem. Eng. Res. Des.* **2015**, *95* (October), 150−161.

(3) Nauha, E. K.; Kálal, Z.; Ali, J. M.; Alopaeus, V. Compartmental Modeling of Large Stirred Tank Bioreactors with High Gas Volume Fractions. *Chem. Eng. J.* **2018**, *334*, 2319−2334.

(4) Vrábel, P.; van Der Lans, R. G. J. M.; Luyben, K. C. A. M.; Boon, L.; Nienow, A. W. Mixing in Large-Scale Vessels Stirred with Multiple Radial or Radial and Axial up-Pumping Impellers: Modelling and Measurements. *Chem. Eng. Sci.* **2000**, *55* (23), 5881−5896.

(5) Kaskiala, T. *Studies on Gas-Liquid Mass Transfer in Atmospheric Leaching of Sulphidic Zinc Concenrtates*; Helsinki University of Technology, 2005.

(6) Tervasmäki, P.; Latva-Kokko, M.; Taskila, S.; Tanskanen, J. Mass Transfer, Gas Hold-up and Cell Cultivation Studies in a Bottom Agitated Draft Tube Reactor and Multiple Impeller Rushton Turbine Configuration. *Chem. Eng. Sci.* **2016**, *155*, 83−98.

(7) Askew, W. S.; Beckmann, R. B. Heat and Mass Transfer in an Agitated Vessel. *Ind. Eng. Chem. Process Des. Dev.* **1965**, *4* (3), 311−318.

(8) Prasher, B. D.; Wills, G. B. *Ind. Eng. Chem. Process Des. Dev.* **1973**, *12* (3), 351−354.

(9) Linek, V.; Kordač, M.; Fujasová, M.; Moucha, T. Gas-Liquid Mass Transfer Coefficient in Stirred Tanks Interpreted through Models of Idealized Eddy Structure of Turbulence in the Bubble Vicinity. *Chem. Eng. Process.* **2004**, *43* (12), 1511−1517.

(10) Morchain, J.; Gabelle, J. C.; Cockx, A. A Coupled Population Balance Model and CFD Approach for the Simulation of Mixing Issues in Lab-Scale and Industrial Bioreactors. *AIChE J.* **2014**, *60* (1), 27−40.

(11) Schwarz, M. P.; Koh, P. T. L.; Verrelli, D. I.; Feng, Y. Sequential Multi-Scale Modelling of Mineral Processing Operations, with Application to Flotation Cells. *Miner. Eng.* **2016**, *90*, 2−16.

(12) Nikolic, D. D.; Frawley, P. J. Application of the Lagrangian Meshfree Approach to Modelling of Batch Crystallisation: Part I-Modelling of Stirred Tank Hydrodynamics. *Chem. Eng. Sci.* **2016**, *145*, 317−328.

(13) Duan, X.; Feng, X.; Yang, C.; Mao, Z. CFD Modeling of Turbulent Reacting Flow in a Semi-Batch Stirred-Tank Reactor. *Chin. J. Chem. Eng.* **2018**, *26*, 675−683.

(14) Haringa, C.; Deshmukh, A. T.; Mudde, R. F.; Noorman, H. J. Euler-Lagrange Analysis towards Representative down-Scaling of a 22 m3 Aerobic S. Cerevisiae Fermentation. *Chem. Eng. Sci.* **2017**, *170*, 653−669.

(15) Haringa, C.; Tang, W.; Wang, G.; Deshmukh, A. T.; van Winden, W. A.; Chu, J.; van Gulik, W. M.; Heijnen, J. J.; Mudde, R. F.; Noorman, H. J. Computational Fluid Dynamics Simulation of an Industrial P. Chrysogenum Fermentation with a Coupled 9-Pool Metabolic Model: Towards Rational Scale-down and Design Optimization. *Chem. Eng. Sci.* **2018**, *175*, 12−24.

(16) Lane, G. L. Improving the Accuracy of CFD Predictions of Turbulence in a Tank Stirred by a Hydrofoil Impeller. *Chem. Eng. Sci.* **2017**, *169*, 188−211.

(17) Enfors, S. O.; Jahic, M.; Rozkov, A.; Xu, B.; Hecker, M.; Jürgen, B.; Krüger, E.; Schweder, T.; Hamer, G.; O'Beirne, D.; et al. Physiological Responses to Mixing in Large Scale Bioreactors. *J. Biotechnol.* **2001**, *85* (2), 175−185.

(18) Paul, E. L.; Atiemo-obeng, V.; Kresta, S. M. *Handbook of Industrial Mixing Science and Practice*; 2004.

(19) Lapin, A.; Müller, D.; Reuss, M. Dynamic Behavior of Microbial Populations in Stirred Bioreactors Simulated with Euler−Lagrange Methods: Traveling along the Lifelines of Single Cells †. *Ind. Eng. Chem. Res.* **2004**, *43* (16), 4647−4656.

(20) Lapin, A.; Schmid, J.; Reuss, M. Modeling the Dynamics of E. Coli Populations in the Three-Dimensional Turbulent Field of a Stirred-Tank Bioreactor-A Structured-Segregated Approach. *Chem. Eng. Sci.* **2006**, *61* (14), 4783−4797.

(21) Tervasmäki, P.; Latva-Kokko, M.; Taskila, S.; Tanskanen, J. Effect of Oxygen Transfer on Yeast Growth Kinetic and Reactor Model to Estimate Scale-up Effects in Bioreactors. *Food Bioprod. Process.* **2018**.

(22) Outotec. Outotec ® Reactor technologies OKTOP Reactor − the complete solution for your process needs http://www.outotec.com/en/Search-material/Search-material-by-categories/?quicksearchquery=reactor&excludeimages=true&categories=68,75.

(23) Gradov, D. V.; Laari, A.; Turunen, I.; Koiranen, T. Experimentally Validated CFD Model for Gas-Liquid Flow in a Round-Bottom Stirred Tank Equipped with Rushton Turbine. *Int. J. Chem. React. Eng.* **2016**, *15* (2).

(24) Hashemi, N.; Ein-Mozaffari, F.; Upreti, S. R.; Hwang, D. K. Analysis of Power Consumption and Gas Holdup Distribution for an Aerated Reactor Equipped with a Coaxial Mixer: Novel Correlations for the Gas Flow Number and Gassed Power. *Chem. Eng. Sci.* **2016**, *151*, 25−35.

(25) Schiller, L.; Naumann, Z. A Drag Coefficient Correlation. *Z.Ver.Deutsch.Ing* **1933**, *77* (13−14), 318−320.

(26) Brucato, A.; Grisafi, F.; Montante, G. Particle Drag Coefficients in Turbulent Fluids. *Chem. Eng. Sci.* **1998**, *53* (18), 3295−3314.

(27) Lane, G. L.; Schwarz, M. P.; Evans, G. M. Numerical Modelling of Gas-Liquid Flow in Stirred Tanks. *Chem. Eng. Sci.* **2005**, *60* (8−9 SPEC. ISS.), 2203−2214.

(28) Roghair, I.; Lau, Y. M.; Deen, N. G.; Slagter, H. M.; Baltussen, M. W.; Van Sint Annaland, M.; Kuipers, J. A. M. On the Drag Force of Bubbles in Bubble Swarms at Intermediate and High Reynolds Numbers. *Chem. Eng. Sci.* **2011**, *66* (14), 3204−3211.

(29) Kawase, Y.; Halard, B.; Moo-Young, M. Liquid-Phase Mass Transfer Coefficients in Bioreactors. *Biotechnol. Bioeng.* **1992**, *39* (11), 1133−1140.
(30) Han, P.; Bartels, D. M. Temperature Dependence of Oxygen Diffusion in H2O and D2O. *J. Phys. Chem.* **1996**, *100* (13), 5597−5602.
(31) Garcia-Ochoa, F.; Gomez, E. Mass Transfer Coefficient in Stirred Tank Reactors for Xanthan Gum Solutions. *Biochem. Eng. J.* **1998**, *1*, 1−10.
(32) Calderbank, P. H.; Moo-Young, M. B. The Continuous Phase Heat and Mass Transfer Properties of Dispersions. *Chem. Eng. Sci.* **1995**, *50* (24), 3921−3934.
(33) Machon, V.; Pacek, A. W.; Nienow, A. W. Bubble Sizes in Electrolyte and Alcohol Solutions in a Turbulent Stirred Vessel. *Chem. Eng. Res. Des.* **1997**, *75* (3), 339−348.
(34) Hu, B.; Pacek, A. W.; Stitt, H. E.; Nienow, A. W. Bubble Sizes in Agitated Air-Alcohol Systems with and without Particles: Turbulent and Transitional Flow. *Chem. Eng. Sci.* **2005**, *60* (22), 6371−6377.
(35) Haringa, C.; Tang, W.; Deshmukh, A. T.; Xia, J.; Reuss, M.; Heijnen, J. J.; Mudde, R. F.; Noorman, H. J. Euler-Lagrange Computational Fluid Dynamics for (Bio)reactor Scale down: An Analysis of Organism Lifelines. *Eng. Life Sci.* **2016**, *16* (7), 652−663.
(36) Lide, D. R. *CRC Handbook of Chemistry and Physics*, 84th Edition, 2003−2004; Vol. *53*, p. 2616.
(37) Joshi, J. B.; Nere, N. K.; Rane, C. V.; Murthy, B. N.; Mathpati, C. S.; Patwardhan, A. W.; Ranade, V. V. CFD Simulation of Stirred Tanks: Comparison of Turbulence Models. Part I: Radial Flow Impellers. *Can. J. Chem. Eng.* **2011**, *89* (1), 23−82.
(38) Gradov, D. V.; González, G.; Vauhkonen, M.; Laari, A.; Koiranen, T. Experimental and Numerical Study of Multiphase Mixing Hydrodynamics in Batch Stirred Tank Applied to Ammoniacal Thiosulphate Leaching of Gold. *J. Chem. Eng. Process Technol.* **2017**, *8* (3), 1−17.
(39) Kalitzin, G.; Medic, G.; Iaccarino, G.; Durbin, P. Near-Wall Behavior of RANS Turbulence Models and Implications for Wall Functions. *J. Comput. Phys.* **2005**, *204* (1), 265−291.
(40) Li, D.; Gao, Z.; Buffo, A.; Podgorska, W.; M, D. L. Droplet Breakage and Coalescence in Liquid−Liquid Dispersions: Comparison of Different Kernels with EQMOM and QMOM. *AIChE J.* **2017**, *63* (6), 2293−2311.
(41) Delafosse, A.; Collignon, M. L.; Crine, M.; Toye, D. Estimation of the Turbulent Kinetic Energy Dissipation Rate from 2D-PIV Measurements in a Vessel Stirred by an Axial Mixel TTP Impeller. *Chem. Eng. Sci.* **2011**, *66* (8), 1728−1737.
(42) Ben-Nun, R.; Sheintuch, M.; Kysela, B.; Konfršt, J.; Fořt, I. Semianalytical Characterization of Turbulence from Radial Impellers, with Experimental and Numerical Validation. *AIChE J.* **2015**, *61* (4), 1413−1426.
(43) Moilanen, P.; Laakkonen, M.; Aittamaa, J. CFD Modelling of Local Bubble Size Distributions in Agitated Gas-Liquid Vessels - Verification against Experiments, 2004, Vol. *18*.
(44) Luo, H. Coalescence, Breakup and Liquid Circulation in Bubble Column Reactors, 1993.
(45) Milo, R.; Jorgensen, P.; Moran, U.; Weber, G.; Springer, M. BioNumbers The Database of Key Numbers in Molecular and Cell Biology. *Nucleic Acids Res.* **2010**, *38* (SUPPL.1), 750−753.

DOI: 10.1021/acs.iecr.8b02765
Ind. Eng. Chem. Res. 2018, 57, 13300−13311